The Surface Chemistry and Structure of Colloidal Lead Halide Perovskite Nanocrystals

Sara R. Smock,[1,†] Yunhua Chen,[2,3,†] Aaron J. Rossini,[2,3,] and Richard L. Brutchey[1,]**

1. Department of Chemistry, University of Southern California, Los Angeles, CA 90089, United States
2. U.S. DOE Ames Laboratory, Ames, IA 50011, United States
3. Department of Chemistry, Iowa State University, Ames, IA 50011, United States

CONSPECTUS: Since the initial discovery of colloidal lead halide perovskite nanocrystals, there has been significant interest placed on these semiconductors because of their remarkable optoelectronic properties, including very high photoluminescence quantum yields, narrow size- and composition-tunable emission over a wide color gamut, defect tolerance, and suppressed blinking. These material attributes have made them attractive components for next-generation solar cells, light emitting diodes, low-threshold lasers, single photon emitters, and X-ray scintillators. While a great deal of research has gone into the various applications of colloidal lead halide perovskite nanocrystals, comparatively little work has focused on the fundamental surface chemistry of these materials. While the surface chemistry of colloidal semiconductor nanocrystals is generally affected by their particle morphology, surface stoichiometry, and organic ligands that

contribute to the first coordination sphere of their surface atoms, these attributes are markedly different in lead halide perovskite nanocrystals because of their ionicity.

In this Account, emerging work on the surface chemistry of lead halide perovskite nanocrystals is highlighted, with a particular focus placed on the most-studied composition of $CsPbBr_3$. We begin with an in-depth exploration of the native surface chemistry of as-prepared, 0-D cuboidal $CsPbBr_3$ nanocrystals, including an atomistic description of their surface termini, vacancies, and ionic bonding with ligands. We then proceed to discuss various post-synthetic surface treatments that have been developed to increase the photoluminescence quantum yields and stability of $CsPbBr_3$ nanocrystals, including the use of tetraalkylammonium bromides, metal bromides, zwitterions, and phosphonic acids, and how these various ligands are known to bind to the nanocrystal surface. To underscore the effect of post-synthetic surface treatments on the application of these materials, we focus on lead halide perovskite nanocrystal-based light emitting diodes, and the positive effect of various surface treatments on external quantum efficiencies. We also discuss the current state-of-the-art in the surface chemistry of 1-D nanowires and 2-D nanoplatelets of $CsPbBr_3$, which are more quantum confined than the corresponding cuboidal nanocrystals but also generally possess a higher defect density because of their increased surface area-to-volume ratios.

KEY REFERENCES

• Cottingham, P.; Brutchey, R. L. On the Crystal Structure of Colloidally Prepared $CsPbBr_3$ Quantum Dots. *Chem. Commun.* **2016**, *52*, 5246–5249.[1] *This study used a combination of synchrotron X-ray diffraction and total scattering techniques to unequivocally assign the phase of colloidal $CsPbBr_3$ nanocrystals as orthorhombic (Pnma).*

• Hanrahan, M. P.; Men, L.; Rosales, B. A.; Vela, J.; Rossini, A. J. Sensitivity-Enhanced ^{207}Pb Solid-State NMR Spectroscopy for the Rapid, Non-Destructive Characterization of Organolead Halide Perovskites. *Chem. Mater.* **2018**, *30*, 7005-7015.[2] *This paper describes how dynamic nuclear polarization (DNP), cryogenic temperatures, or fast magic angle spinning and proton detection can be used to enhance the sensitivity of ^{207}Pb solid-state NMR experiments on lead halide perovskites.*

• Smock, S. R.; Williams, T. J.; Brutchey, R. L. Quantifying the Thermodynamics of Ligand Binding to $CsPbBr_3$ Quantum Dots. *Angew. Chem. Int. Ed.* **2018**, *57*, 11711-11715.[3] *Solution ^{1}H NMR was used to quantify the thermodynamics of ligand exchange of $CsPbBr_3$ nanocrystals with carboxylic acids, primary amines, and phosphonic acids. Increases in nanocrystal steady-state PL intensities correlated with the addition of more strongly bound anionic ligands.*

• Chen, Y.; Smock, S. R.; Flintgruber, A. H.; Perras, F. A.; Brutchey, R. L.; Rossini, A. J. Surface Termination of $CsPbBr_3$ Perovskite Quantum Dots Determined by Solid-State NMR Spectroscopy. *J. Am. Chem. Soc.* **2020**, *142*, 6117-6127.[4] *This report used solid-state NMR spectroscopy to verify the CsBr surface termination of cuboidal $CsPbBr_3$ nanocrystals and that alkylammonium cations occupy Cs surface positions.*

1. INTRODUCTION

Perovskites are any material in the same structure type family as the mineral $CaTiO_3$, which was discovered in 1839 and named after the Russian mineralogist Lev Perovski.[5] Over the past 100 years, the ABO_3 oxide perovskites (A=12-coordinate cation, B=6-coordinate cation), where the $[BO_6]$ octahedra are linked by corner sharing in three dimensions, have been intensively studied because of their multifunctionality.[6] The perovskite structure class can be more broadly defined as ABX_3,[7] where the X anion can also be a chalcogenide (e.g., $BaZrS_3$),[8] a pnictide (e.g., $LaWN_3$),[9]

or a halide (e.g., $CsPbX_3$, X=Cl, Br, I).[10] The ABX_3 halide perovskites, while known since the late nineteenth century,[11] have undergone a renaissance because of the remarkable photovoltaic performance of $MAPbI_3$-based thin films (MA=methylammonium). Lead halide perovskite solar absorbers have garnered massive attention because of their high power conversion efficiencies (PCEs), currently >25%.[12] These performance achievements have partly been enabled by post-deposition treatments for chemical passivation. Treatment with Lewis bases (e.g., pyridine,[13] phosphine oxide[14]) and alkylammonium halides (e.g., methylammonium iodide,[15] ethylammonium iodide[16]) help minimize non-radiative recombination and enhance device performance; however, an atomistic understanding of how these passivants coordinate to the surface is often lacking. The small surface area-to-volume ratio of large grained polycrystalline halide perovskites obscure these efforts.

Colloidal lead halide perovskite nanocrystals, on the other hand, have large surface area-to-volume ratios because of their small size, which increases the importance of their surfaces on ensuing optoelectronic properties, making them an ideal platform for studying surface chemistry. Approximately 20% of the atoms in a 10 nm $CsPbBr_3$ nanocrystal are within the first surface layer of the particle. The surface chemistry of semiconductor nanocrystals is affected by their exposed crystal facets,[17,18] stoichiometry,[19,20] organic ligands,[21–23] and ionicity.[24–26] Unlike more covalent semiconductor nanocrystals (e.g., CdSe, InP), lead halide perovskites are markedly ionic, which affects their environmental stability,[27] electronic structure and defect tolerance,[28] and ligand binding and fluxionality.[29] These unique characteristics make lead halide perovskite nanocrystals a rich area of study, with the all-inorganic $CsPbX_3$ nanocrystals being the most studied because of their excellent optoelectronic properties, including size- and composition-dependent band gaps, high photoluminescence quantum yields (PLQYs), narrow emission line widths that cover a wide

color gamut, and suppressed blinking.[30,31] These properties make $CsPbX_3$ nanocrystals appealing for use in optical devices; for example, solar cells, low threshold lasers, light emitting diodes (LEDs), single photon emitters, and X-ray scintillators.[32]

In 2014, Galian and Pérez-Prieto reported the first low-temperature synthesis of colloidal halide perovskite nanocrystals through a ligand assisted reprecipitation technique, whereby $MAPbBr_3$ nanocrystals were prepared through the rapid mixing of cation and bromide precursors to induce precipitation of the halide perovskite in the presence of long-chain capping ligands, which arrest growth.[33] Variants of this method were later applied to the room-temperature synthesis of colloidal $CsPbX_3$ nanocrystals.[34] Following this initial work, Kovalenko synthesized $CsPbX_3$ nanocrystals by the hot-injection of a Cs(oleate) solution in 1-octadecene into a solution of PbX_2, oleic acid, and oleylamine at 140-200 °C.[35] This synthesis results in morphologically well-defined cuboidal nanocrystals ranging in edge length from 4-15 nm and has become the prototypical preparation method for 0-D $CsPbX_3$ nanocrystals. The PL emission wavelength can be tuned by varying nanocrystal size and composition (**Figure 1**).

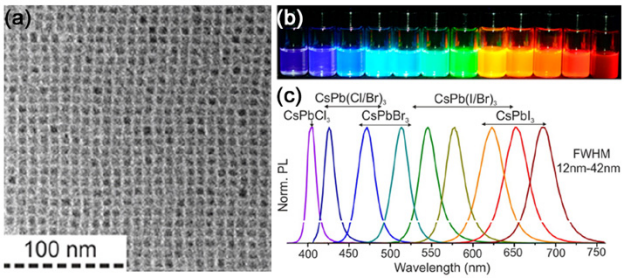

Figure 1. (a) TEM micrograph of 0-D $CsPbBr_3$ nanocrystals. (b) Colloidal suspensions of $CsPbX_3$ (X=Cl, Br, I) nanocrystals under UV excitation. (c) PL spectra of $CsPbX_3$ (X=Cl, Br, I) nanocrystal suspensions. Reproduced with permission from ref. 35. Copyright (2015) American Chemical Society.

2. CUBOIDAL 0-D $CsPbBr_3$ NANOCRYSTALS

Native Surface Chemistry of $CsPbBr_3$ Nanocrystals. Understanding the surface chemistry of halide perovskite nanocrystals is crucial to rationally improving and tuning their photophysical

properties. Prior to discussing structural features of the $CsPbBr_3$ nanocrystal surface, it is necessary to understand the bulk structure. Using both Rietveld refinement and pair distribution function analyses of X-ray total scattering data, Brutchey and co-workers determined that the crystal structure of colloidal 9 nm $CsPbBr_3$ nanocrystals is orthorhombic (*Pnma*)[1,36] up until a temperature of 50 ˚C < $T_{\gamma-\beta}$ < 59 ˚C, where a transition to a tetragonal phase (*P*4/*mbm*) occurs, followed by a higher-temperature transition to the cubic ($Pm\bar{3}m$) phase at 108 ˚C < $T_{\beta-\alpha}$ < 117 ˚C.[37] The 0-D $CsPbBr_3$ nanocrystals obtained by the Protesescu hot-injection method typically adopt a cuboidal morphology, whereby the (001) and (110) facets have been predicted to be terminate the nanocrystal surface.[28] Given this crystal structure and particle morphology, two types of surfaces can occur – a CsBr terminated surface and a $PbBr_2$ terminated surface. In recent experimental reports, high-resolution TEM (HR-TEM) images revealed that cuboidal $CsPbBr_3$ nanocrystals exhibit (001) and (110) crystal lattice planes that compose the surface facets of these particles.[38–40]

Given the high fraction of atoms that reside at the surface of nanocrystals, measuring the particle elemental stoichiometry gives insight into the surface composition.[19,20] Ravi et al. applied variable energy X-ray photoelectron spectroscopy (XPS) to probe the composition of 10 nm $CsPbBr_3$ nanocrystals in a layer-by-layer fashion,[40] and found that the Br:Cs elemental ratio is ~5 at the surface of the $CsPbBr_3$ nanocrystals and decreases to the expected ratio of ~3 in the bulk which clearly suggests a surface excess of Br. However, if some of the surface Cs-sites were occupied by alkylammonium cations a Br:Pb ratio of >3 and a Cs:Pb ratio of ~1 could arise for a CsBr termination. Kovalenko and Infante computationally predicted that the Br:Pb ratio should be ca. 3.2 for CsBr terminated $CsPbBr_3$ nanocrystals in the size range of 7-11 nm (**Figure 2**). They confirmed this prediction experimentally using inductively coupled plasma-optical emission

spectroscopy (ICP-OES), demonstrating that 9 nm $CsPbBr_3$ nanocrystals give Br:Pb ratios of 3.2-3.5.[41] Kovalenko and Infante also suggested that $PbBr_2$ termination of the cuboidal $CsPbBr_3$ nanocrystals is unlikely because it requires a much denser ligand packing, which would encounter significant steric hindrance, and disruption of the Pb^{2+} octahedral coordination.

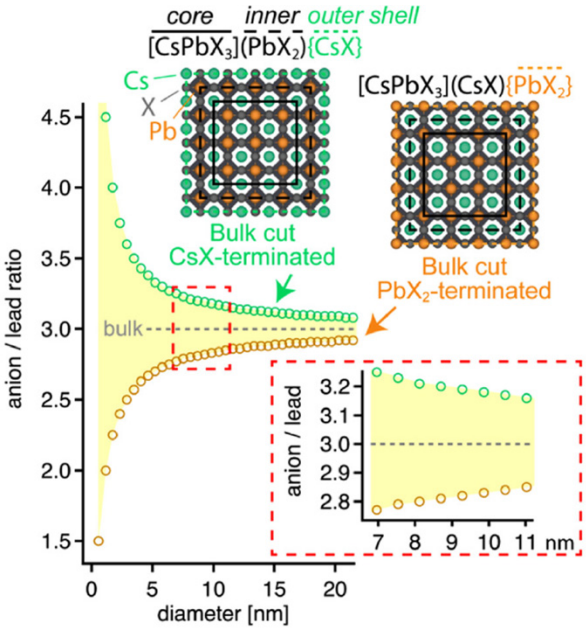

Figure 2. Size-dependent anion/lead ratio of cuboidal $CsPbX_3$ nanocrystals. The inset shows the anion/lead ratio for experimentally observed nanocrystal sizes. Reproduced with permission from ref. 41. Copyright (2019) American Chemical Society.

CsBr termination of the $CsPbBr_3$ nanocrystals was confirmed by Rossini and Brutchey using solid-state NMR spectroscopy.[4] ^{1}H detected fast magic angle spinning (MAS) were used to enhance the sensitivity of surface-selective ^{14}N, ^{133}Cs and ^{207}Pb NMR experiments.[2] Surface-selective ^{133}Cs solid-state NMR spectra show the presence of an additional ^{133}Cs NMR signal, suggesting that Cs ions reside on the surface. ^{1}H-^{133}Cs and ^{1}H-^{207}Pb inter-nuclear distance measurements between dodecylammonium $-NH_3^+$ ligand protons and surface and subsurface ^{133}Cs and ^{207}Pb spins indicates the particles are CsBr terminated with alkylammonium ligands substituted into some surface A-sites (**Figure 3**). The positioning of alkylammonium ligands in surface A-sites is akin to alkylammonium positions in 2-D Ruddlesden–Popper phases[42] and

consistent with the proposed model of Ravi et al.[40] A CsX surface termination is also consistent with a HAADF-STEM analysis of cuboidal $CsPbI_3$ nanocrystals that showed CsI termination.[43] Cuboidal $CsPbI_3$ nanocrystals possess a orthorhombic crystal structure isostructural with $CsPbBr_3$.[44]

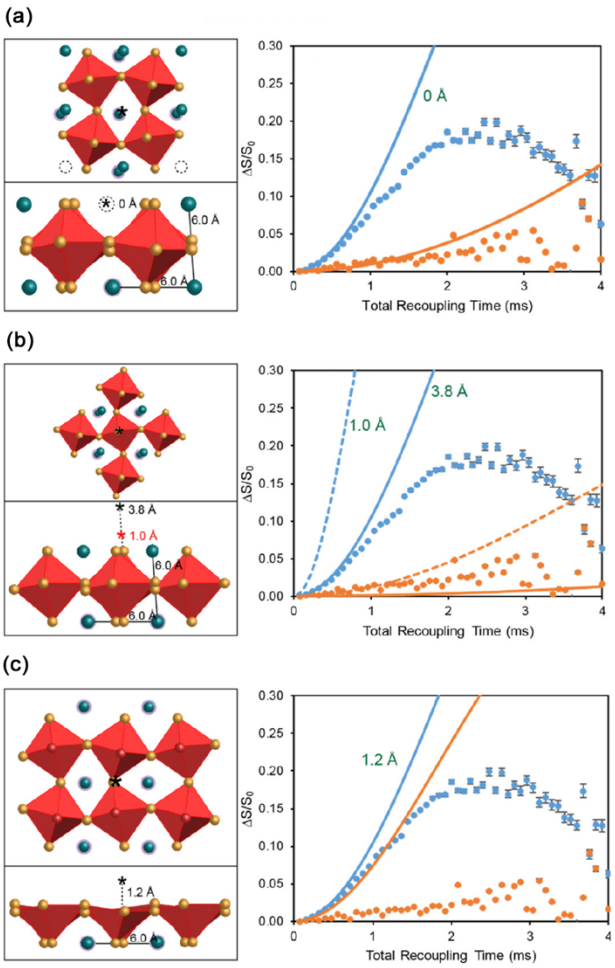

Figure 3. Models of the orthorhombic (010) $CsPbBr_3$ surface showing (a) CsBr termination with alkylammonium substitution at surface Cs-sites, (b) CsBr termination without alkylammonium substitution, and (c) $PbBr_2$ termination. The asterisk indicates the position of an alkylammonium H atom. Blue spheres with and without a purple halo correspond to subsurface and surface Cs atoms, respectively. Experimental $\Delta S/S_0$ intensities were plotted as a function of total recoupling time for $CsPbBr_3$ nanocrystals. Blue points correspond to $^{1}H\{^{133}Cs\}$ RESPDOR and orange points correspond to $^{1}H\{^{207}Pb\}$ S-REDOR experiments. Simulated dephasing curves are depicted with blue and orange lines. Reproduced with permission from ref. 4. Copyright (2020) American Chemical Society.

The native ligands on $CsPbBr_3$ nanocrystal surfaces consist of long-chain primary alkylammonium ligands (oleylammonium) and long-chain carboxylate ligands (oleate). Considering a pseudo-cubic lattice parameter (0.587 nm), a theoretical monolayer value of 5.8 ligands nm^{-2} was previously calculated for $CsPbBr_3$ assuming that the surface is solely passivated by inorganic CsBr atoms.[29] However, for long-chain organic ligands with 0.3−0.5 nm^2 $ligand^{-1}$ footprints,[3,45] the maximum allowable ligand density is on the order of 2−3 ligands nm^{-2}.[4] Indeed, most measured values of native ligand densities of $CsPbBr_3$ nanocrystals fall within this range.[3,4,29]

The native ligands affect particle morphology,[38] stability,[46] and solution dispersibility, and also passivate electronic trap states. However, the native surface ligands are labile, even in nonpolar solvents, which contributes to the poor stability of $CsPbX_3$ nanocrystals.[29] The dynamic equilibrium of ligand binding to $CsPbBr_3$ nanocrystals was quantified using solution ^{1}H NMR spectroscopy by Brutchey et al.[3] The native oleylammonium and oleate ligands dynamically exchange with free alkylamines and carboxylic acids in solution. The exchange of native oleate with 10-undecenoic acid is exergonic, with positive ΔH and positive ΔS, and this exchange is favorable at room temperature or higher. The exchange of native oleylammonium with 10-undeceneamine is also exergonic at room temperature, but with a negative ΔH and negative ΔS, suggesting this exchange will become less favorable with elevated temperatures. Giansante and co-workers explored a library of amine ligands with variable pK_b, steric hindrance, and chain length with the goal of achieving thermodynamically stable surface coordination and effective passivation by exchange of native amine ligands on $CsPbBr_3$ nanocrystals.[47] For oleylammonium-capped $CsPbBr_3$ nanocrystals, the stoichiometric addition of short (C4-C8), strongly basic primary alkylamines results in binding to the nanocrystal surface after proton transfer from free oleylammonium in solution to improve colloidal stability and give near-unity PLQYs.

Post-Synthetic Surface Treatments. Didodecyldimethylammonium bromide (DDAB), a quaternary ammonium salt, has been shown to be a very effective passivating ligand for $CsPbBr_3$ nanocrystals. Further, the charge of DDAB is pH independent. Manna et al. demonstrated that the post-synthetic addition of DDAB to $CsPbBr_3$ nanocrystals with native Cs-oleate ligands results in superior colloidal stability and near-unity PLQYs (**Figure 4**).[48] They hypothesize that these beneficial effects result from weaker ligand-solvent interactions for DDAB over Cs-oleate, which drives the quaternary ammonium salt to the nanocrystal surface. Manna and Krahne followed this initial work with a temperature-dependent PL study comparing $CsPbBr_3$ nanocrystals treated with DDAB versus nanocrystals with Cs-oleate or oleylammonium oleate on their surface.[49] The photophysics of the DDAB-treated sample was found to behave differently; the time-resolved PL spectra maintained monoexponential decay down to low temperatures and the PL spectrum at 4 K possessed significantly less low-energy tailing. The authors hypothesized that DDAB-treated $CsPbBr_3$ nanocrystals have a lower trap state density resulting from more efficient surface passivation.

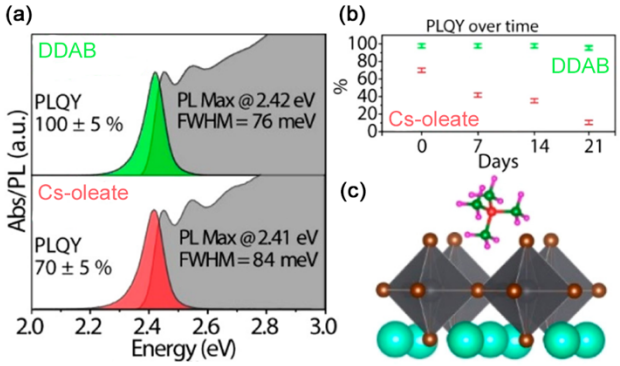

Figure 4. (a) Absorbance and PL spectra of Cs-oleate (red) and DDAB (green) capped $CsPbBr_3$ nanocrystals. (b) Evolution of PLQY for the two types of $CsPbBr_3$ nanocrystals. (c) Model of tetramethylammonium bromide sitting in the A-site of $CsPbBr_3$. Reproduced with permission from ref. 48. Copyright (2019) American Chemical Society.

Kovalenko and Infante showed that post-synthetic ligand treatment of $CsPbBr_3$ nanocrystals with DDAB and $PbBr_2$ significantly increases the PLQY from 60-70% (for the as-prepared nanocrystals with oleic acid and oleylamine) to 90-100% post-treatment.[41] The authors performed both DDAB and $PbBr_2$ and DDAB-only ligand treatments and found that the combination of both DDAB and $PbBr_2$ resulted in a 10-20% higher PLQY and prolonged colloidal stability. The authors rationalized the improved PLQY and colloidal stability to result from the combination of $PbBr_2$ for "healing" of the ($PbBr_2$) nanocrystal surface layer, presumably through passivation of bromine vacancies (V_{Br}), and superior steric stabilization by DDAB. Despite the positive effects of DDAB treatments on PLQY and colloidal stability, there are still outstanding issues. Manna and Krahne noted that the PL intensity of DDAB-treated $CsPbBr_3$ nanocrystals decreases with increasing temperature from 250 K to room temperature, suggesting that more thermally robust ligand passivation is needed for device applications working above room temperature.[49] Additionally, Giansante et al. reported spectrophotometric data that suggest nanocrystal restructuring upon the addition of substoichiometric amounts of DDAB.[47] An atomistic understanding of this restructuring based on empirical evidence is currently missing.

Zwitterionic ligands have become an interesting and effective strategy for stabilization and surface passivation. Zwitterions have two advantages over traditional oleylammonium oleate ligands: (i) zwitterions contain both cationic and anionic groups and there is no chance of neutralization by Brønsted acid-base equilibria, and (ii) ligand binding is stabilized by the chelate effect.[50,51] Kovalenko et al. explored commercially available zwitterions (i.e., sulfobetaines, phosphocholines, γ-amino acids) for passivation of $CsPbBr_3$ nanocrystals (**Figure 5**). They found that sulfobetaine-capped $CsPbBr_3$ nanocrystals formed more concentrated suspensions (50-100 mg mL^{-1}), remained more colloidally stable upon several washing cycles with polar nonsolvents, and

retained higher PLQYs for extended periods, as compared to standard oleate- and oleylammonium-capped $CsPbBr_3$ (**Figure 5c**). DFT calculations were used to study sulfobetaine binding to a $CsPbBr_3$ nanocrystal surface and compare against oleylammonium bromide and oleylammonium oleate binding. The anionic sulfonate group of sulfobetaine binds to sub-surface Pb (similar to bromide and oleate), while the cationic quaternary ammonium group of sulfobetaine occupies surface A-site vacancies (similar to oleylammonium). The quaternary ammonium group of sulfobetaine is still well accommodated into the A-site, despite its steric bulk. The binding energies for the traditional ligand ion pairs and the sulfobetaine zwitterion were comparable (40-45 kcal mol^{-1}), suggesting that the improved properties are a result of the chelate effect.

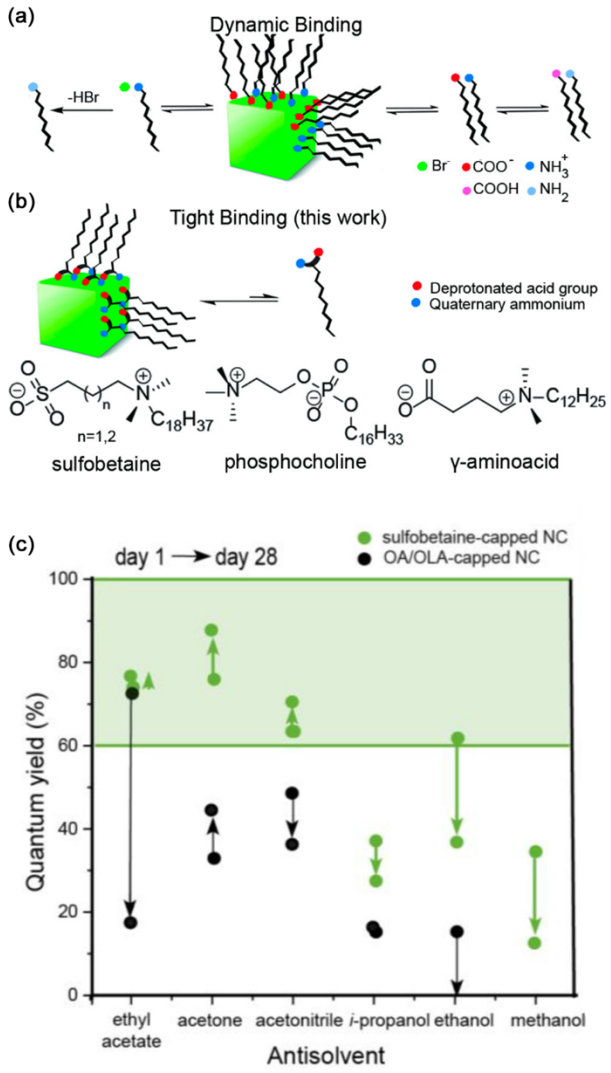

Figure 5. (a) Graphical depiction of as-prepared $CsPbBr_3$ nanocrystals capped with traditional long-chain ligands (oleate or bromide and oleylammonium), and (b) with zwitterions containing both cationic and anionic groups in one molecule. (c) PLQY of $CsPbBr_3$ nanocrystals terminated with 3-(*N*,*N*-dimethyloctadecylammonio)propanesulfonate (green) and oleylammonium oleate (black) ligands after a two-step of purification on day 1 and after day 28. Reproduced with permission from ref. 50. Copyright (2018) American Chemical Society.

Kovalenko et al. further examined the utility of soy lecithin, a natural phospholipid, which contains a physical mixture of zwitterions with various combinations of both saturated and unsaturated hydrocarbon chains. Soy lecithin binds to the nanocrystal surface through both quaternary ammonium and dialkylphosphate functionalities resulting in tighter ligand binding and superior colloidal stability as compared to standard oleylammonium oleate ligands, allowing for a

wide range of colloid concentrations ranging from ultradilute (ng/mL) to ultraconcentrated conditions (>400 mg/mL).[52] The authors rationalized the high colloidal stability of the lecithin-stabilized $CsPbBr_3$ nanocrystals using the Alexander-De Gennes model of polymeric interactions, which attributes the increased colloidal stability to increased particle-particle repulsion resulting from the tight ligand binding, high grafting density (1.8 nm^{-2}), and ligand chain polydispersity.[53–55] The resulting lecithin-stabilized $CsPbBr_3$ nanocrystals demonstrated high PLQYs, equal to or better than the aforementioned first-generation zwitterions.

Oleic acid has been replaced with other long-chain Brønsted acids, such as alkylphosphonic acids, to stabilize $CsPbX_3$ nanocrystals. Alkylphosphonates bind tightly to $CsPbBr_3$ nanocrystals, allowing for excellent surface passivation, improved PLQYs, and superior colloidal stability.[56,57] Undercoordinated surface lead atoms are a cause of surface trap states for $CsPbX_3$ nanocrystals and due to the relatively soft Lewis acid character of lead, a complementary soft Lewis base, such as a phosphonate, is highly effective for surface passivation.[58] Alivisatos and co-workers found addition of hexylphosphonic acid improved the PLQY from 76% (with a native ligand shell of oleylammonium oleate) to 98% (with a ligand shell of oleylammonium hexylphosphonate) for $CsPbBr_3$ nanocrystals.[58] In a separate study, Brutchey et al. used solution ^1H NMR spectroscopy to show that an alkenylphosphonic acid (10-undecylphosphonic acid) irreversibly binds and displaces oleic acid from the $CsPbBr_3$ nanocrystal surface, quantitatively confirming the tighter binding of softer phosphonate ligands over oleate ligands (**Figure 6a**).[3]

Rossini and Brutchey further explored the binding of this same alkenylphosphonate ligand on $CsPbBr_3$ nanocrystals using solid-state NMR spectroscopy.[4] A 2D $^1H \rightarrow ^{31}P$ CP-HETCOR spectrum revealed a narrow ^{31}P NMR signal at 26 ppm coincident with a broader signal that extends to 20 ppm; these ^{31}P NMR peaks correlate with ^1H NMR peaks at 9.5 and 11 ppm that

correspond to acid protons (**Figure 6b**). These data suggest two chemically distinct binding sites on the $CsPbBr_3$ nanocrystals for singly deprotonated phosphonate ligands. The broader ^{31}P signal correlates with a ^{1}H NMR signal at 7.5 ppm assigned to alkylammonium $–NH_3^+$ protons, suggesting some degree of ion pairing between the alkenylphosphonate and alkylammonium ligands. These results agree with a study by Mathews and co-workers that reported a primary ^{31}P peak at 25 ppm for octylphosphonate-capped $CsPbBr_3$ nanocrystals.[59] Based on ^{31}P chemical shifts and HETCOR experiments they assigned this peak to singly deprotonated, monoanionic octylphosphonate that self-assemble into a hydrogen bonded interligand network, which is surmised to contribute to the strong binding of alkylphosphonates. As predicted by Alivisatos and co-workers, soft Lewis base sulfonate ligands also stabilize $CsPbBr_3$ nanocrystals and passivate surface traps.[58] Zeng et al. reported that benzenesulfonate ligands result in $CsPbBr_3$ nanocrystals with high PLQYs (>90%) that maintain structural and optoelectronic stability through eight purification cycles and storage >5 months.[60]

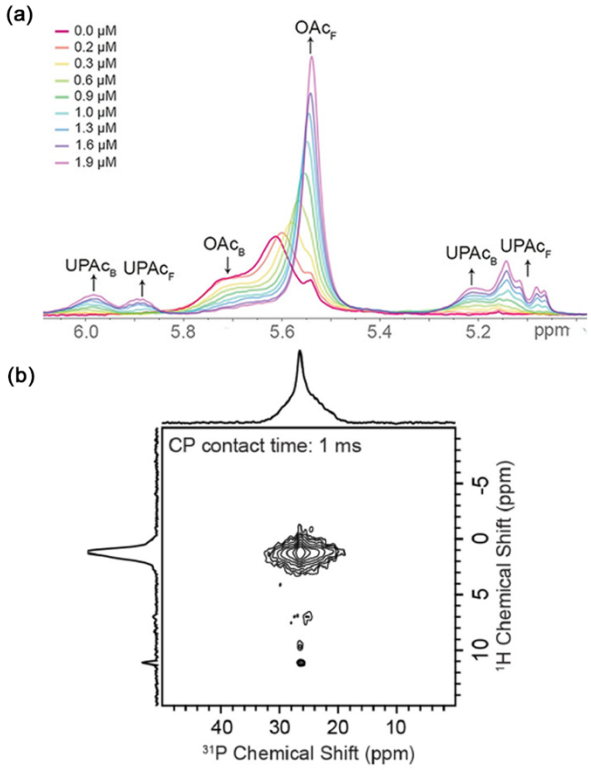

Figure 6. (a) Solution ^{1}H NMR spectra of a $CsPbBr_3$ nanocrystal suspension with oleic acid (OAc) and dodecylamine native ligands, titrated with 10-undecenylphosphonic acid (UPAc) (from 0–1.9 μM), showing free (F) and bound (B) ligands. Reproduced with permission from ref. 3. Copyright (2018) Wiley, (b) 2D dipolar $^{1}H \rightarrow ^{31}P$ CP HETCOR of $CsPbBr_3$ nanocrystals terminated with UPAc. Reproduced with permission from ref. 4. Copyright (2020) American Chemical Society.

Applications of Ligand Exchanged Nanocrystals. While the insulating native ligands are needed for nanocrystal synthesis, colloidal stability, and processing, it is well known that long-chain ligands impede performance in solid-state devices.[61–63] For LEDs, native ligands are needed to passivate surface trap states to improve external quantum efficiencies (EQEs), but simultaneously insulate the nanocrystals from charge injection. Ligand exchange strategies, such as those discussed above, have been employed to facilitate exciton management in halide lead perovskite nanocrystal LEDs, with the goal of passivating surface trap states, reducing the alkyl chain lengths, and reducing ligand density on the nanocrystal surface (e.g., going from primary to quaternary alkylammonium ligands). In 2016, Bakr and Sargent reported an EQE of 3% for green LEDs based on an indium tin oxide (ITO)/poly(ethylenedioxythiophene):polystyrene sulfonate (PEDOT:PSS)/poly(9-vinylcarbazole) (PVK)/$CsPbBr_3$ nanocrystal/2,2',2''-(1,3,5-benzenetriyl) *tris*-[1-phenyl-1H-benzimidazole] (TPBi)/LiF/Al device architecture, where the nanocrystals were treated with DDAB (**Figure 7**).[64] This was a significant improvement over previous $CsPbBr_3$ nanocrystal-based green LEDs that had EQEs of only 0.2% with the insulating native ligands.[65] Sargent et al. followed this initial work with a two-step ligand treatment that further reduced the organic content on the $CsPbBr_3$ nanocrystal surface.[66] Therein, the as-prepared $CsPbBr_3$ nanocrystals were initially treated with isopropylammonium bromide, passivating V_{Br} and significantly reducing the alkylammonium cation size. The colloidal suspension of $CsPbBr_3$ nanocrystals were then treated with NaBr to exchange the isopropylammonium cations with Na^{+}; the authors report the PLQY of the nanocrystal suspension remained unchanged over 6 months,

with the resulting electrostatic stabilization enabled by dimethylformamide, a polar aprotic solvent. Compared to a DDAB surface treatment, the two-step ligand treatment of isopropylammonium bromide followed by NaBr gave 20% higher PLQYs for 7 nm $CsPbBr_3$ nanocrystals, resulting in an EQE of 22% for green LEDs based on an ITO/PEDOT:PSS/poly[bis-(4-phenyl)(2,4,6-trimethylphenyl)amine] (PTAA)/$CsPbBr_3$ nanocrystal/TPBi/LiF/Al device architecture.

Lead halide perovskite nanocrystals have also been used as absorber layers in nanocrystal-based solar cells, with the greatest focus being placed on $CsPbI_3$ nanocrystals because of their narrower band gaps. Again, the $CsPbI_3$ nanocrystal native ligands must be removed to facilitate charge transport in the nanocrystal thin film array. Wheeler and Luther reported PCEs approaching 12% for $CsPbI_3$ nanocrystal-based solar cells facilitated by the exchange of the long-chain oleylammonium oleate native ligands with formamidinium acetate.[67] More recently, Yuan and Ma obtained devices with PCEs approaching 15%,[68] by ligand using a secondary amine (di-*n*-propylamine) to reduce the length of the insulating ligand barrier and the overall ligand density.

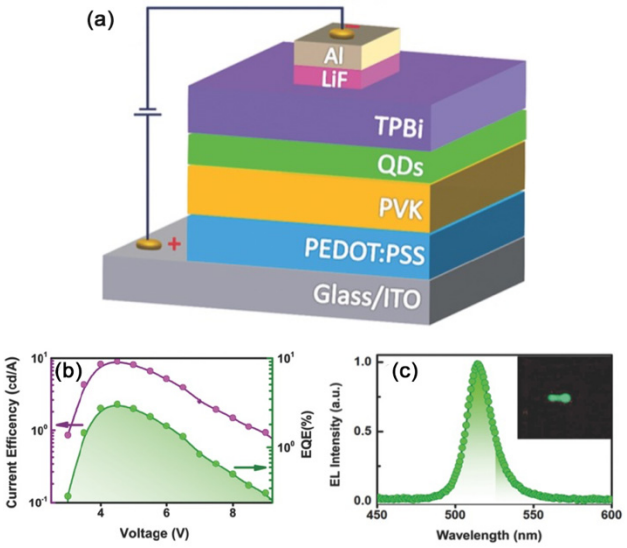

Figure 7. (a) Schematic of perovskite nanocrystal LED device. (b) Current efficiency and EQE versus driving voltage. (c) Electroluminescence spectrum at an applied voltage of 4.5 V (inset: photograph of the device under applied voltage). Reproduced with permission from ref. 64. Copyright (2016) Wiley.

3. 1-D $CsPbBr_3$ NANOWIRES

In 2015, Yang and co-workers reported the solution-phase synthesis of $CsPbX_3$ nanowires prepared by the hot-injection of Cs(oleate) into a solution of PbX_2, oleic acid, and oleylamine in 1-octadecene at 150−250 ˚C.[69] By quenching the reaction at a later stage (40–60 min), they obtained 1-D nanowires with uniform diameters between 10-20 nm and lengths up to 5 μm. Subsequently, Manna and co-workers modified the $CsPbBr_3$ nanowire synthesis by introducing short-chain carboxylic acid ligands to obtain wires with diameters between 3.4-20 nm.[70] Wires with diameters <10 nm exhibited quantum confinement effects, resulting in a blue shift of absorption and emission maxima. In parallel, the Yang and Alivisatos groups prepared ultra-thin 2.2 nm diameter $CsPbBr_3$ nanowires by using anti-solvent purification strategies to post-synthetically separate nanowires from nanocubes.[71] Small-angle X-ray scattering (SAXS) revealed periodic packing of the ultra-thin nanowires, confirming the narrow size distribution of the nanowire diameter, and suggesting deep interpenetration of the ligands. The PLQY of the resulting nanowires was ca. 30%, likely because the 1-D nature of the ultra-thin nanowires results in a high surface area-to-volume ratio. Surface treatment with $PbBr_2$ improved the PLQY in addition to the morphological stability of the nanowires, similar to results for cuboidal $CsPbBr_3$ nanocrystals.

Alternative synthetic approaches have also been developed. Bakr and co-workers reported that visible-light illumination converted 7 nm cuboidal $CsPbBr_3$ nanocrystals into nanowires with diameters >50 nm.[72] Visible-light was proposed to cause photo-induced dissociation of the weakly bound oleylammonium/oleate ligands, resulting in nanocube coalescence. The stability of different surface terminations was hypothesized to cause the anisotropic growth along the [110] direction of the orthorhombic structure (**Figure 8**).

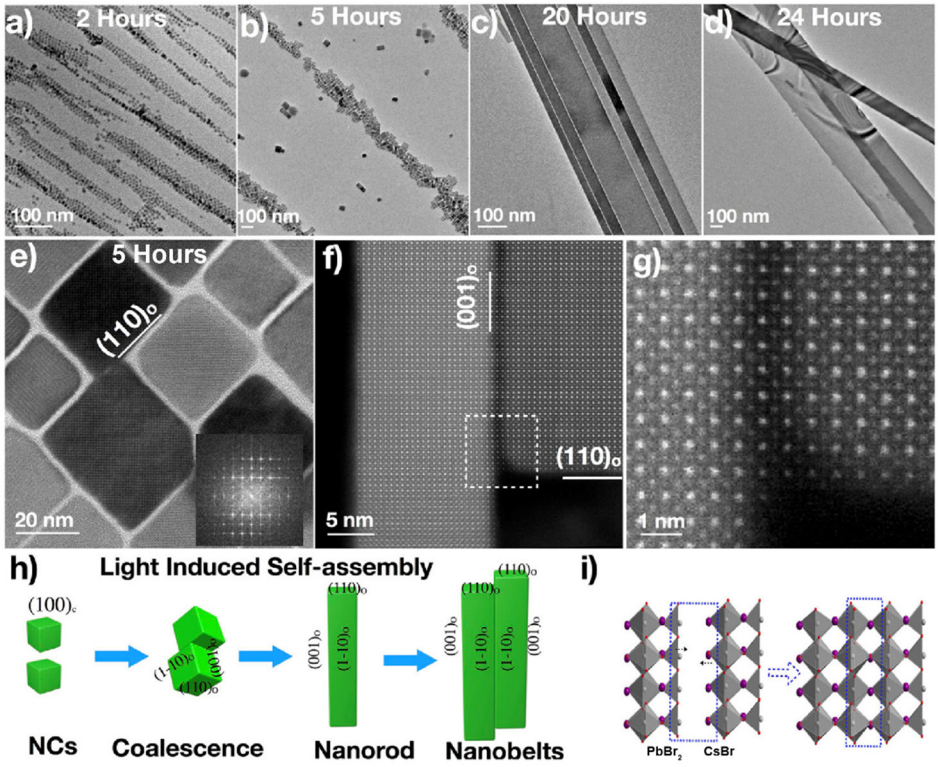

Figure 8. (a–d) Shape evolution of 1-D $CsPbBr_3$ nanowires under illumination for variable times. (e) HRTEM images showing $CsPbBr_3$ nanocrystals (5 h of illumination) coalescing along the $[110]_o$ crystallographic direction. (f) HAADF-STEM image of nanorods acquired along the $[1\bar{1}0]_o$ zone axis, showing an interface between two nanorods that are attached through $(001)_o$ surfaces. (g) Magnification of the selected area in (f). (h) Illustration of light driven conversion of $CsPbBr_3$ nanocrystals. (i) Schematic diagram of half-unit cell fusion process on the CsBr- and $PbBr_2$-terminated $(001)_o$ surfaces. Reproduced with permission from ref. 72. Copyright (2019) American Chemical Society.

4. 2-D $CsPbBr_3$ NANOPLATELETS

While most 0-D $CsPbBr_3$ nanocrystals exhibit bulk-like or weakly confined behavior, very strong quantum confinement can be achieved in 2-D nanoplatelets. In nanoplatelets, the single monolayer (ML) control of thickness can be used to increase the optical band gap, with blue band-edge emission from $CsPbBr_3$ nanoplatelets as compared to green emission from 0-D $CsPbBr_3$ nanocrystals.[73] Correspondingly, halide perovskite nanoplatelets possess much larger exciton binding energies (i.e., 120-280 meV as compared to 40 meV for 10 nm cuboidal particles) and

reduced dielectric screening;[74–77] these characteristics make halide perovskite nanoplatelets of interest for LEDs.[78–80]

$CsPbBr_3$ nanoplatelets can be synthesized by hot-injection,[81,82] ligand assisted reprecipitation,[75] and thermal methods.[83] Control over nanoplatelet thickness can be achieved by tuning various synthetic parameters, such as precursor and ligand ratios,[73,75,84] reaction temperature,[82] and ligand chain length.[38,85,86] While the orthorhombic crystal structure, CsBr surface termination, and alkylammonium carboxylate ligand shell are the same as 0-D cuboidal nanocrystals,[81] the increased surface area-to-volume ratio and surface defect density of the nanoplatelet morphology result in significantly lower PLQYs.[73] As a result, post-synthetic surface treatments have been explored to repair surface traps and increase PLQY (**Figure 9**).[75] The fluxional ligand shell also makes $CsPbBr_3$ nanoplatelets prone to aggregation and growth into larger sheet- and bulk-like structures through temperature- and light-induced processes.[87,88]

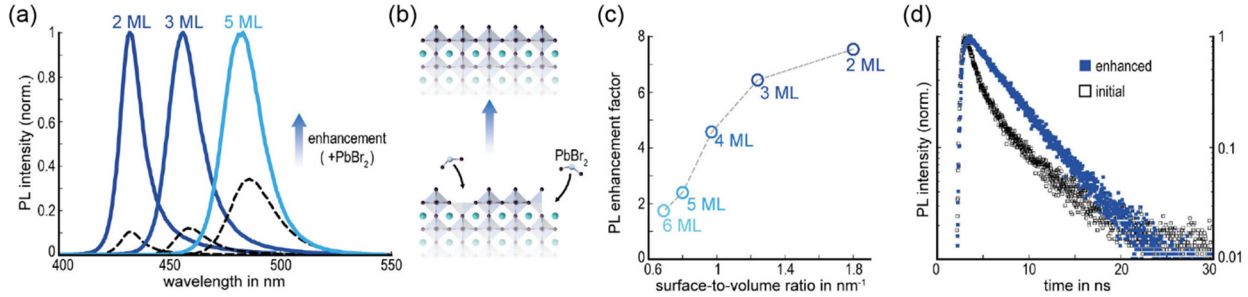

Figure 9. (a) PL spectra of $CsPbBr_3$ nanoplatelet colloidal dispersions before (dashed lines) and after (solid lines) surface-treatment. (b) Scheme for the repair of surface defects initiated by a post-synthetic treatment with $PbBr_2$. (c) PL enhancement factor as a function of the surface-to-volume ratio. (d) Time resolved-PL spectra of 3 ML thick nanoplatelets before (open black squares) and after treatment (full blue squares). Reproduced with permission from ref. 75. Copyright (2018) American Chemical Society.

Urban and Feldmann showed that the PLQY of $CsPbBr_3$ nanoplatelets can be significantly improved by a post-synthetic treatment with $PbBr_2$ in combination with oleic acid and oleylamine.[75] The as-prepared $CsPbBr_3$ nanoplatelets with a 2-ML thickness exhibited a PLQY of

only 7%. After treatment with the $PbBr_2$-ligand solution, the PLQY increased 7-fold; this effect was not observed when only oleic acid and oleylamine were added. The $PbBr_2$ treatment is hypothesized to fill V_{Pb} and V_{Br} on the nanoplatelet surfaces (**Figure 9b**), resulting in enhanced PLQY and lifetimes (**Figures 9c,d**). Rabouw and van der Stam performed an in-depth study of the photophysics of the $CsPbBr_3$ nanoplatelets before and after treatment with the $PbBr_2$-ligand solution.[89] Their findings revealed the presence of a dark fraction of completely nonfluorescent nanoplatelets whereby photogenerated excitons are quenched by ultrafast nonradiative recombination that outcompete thermalization to the band edge. Importantly, they found that this fraction of dark $CsPbBr_3$ nanoplatelets is unaffected by the $PbBr_2$-ligand treatment. In turn, the $PbBr_2$-ligand treatment enhances prompt emission by suppressing carrier trapping at the lowest energy exciton state and decreases the contribution of delayed emission from trapping-detrapping events to the overall nanoplatelet emission. Since nonradiative recombination and trapping-detrapping are both affected by ligand-treatment with $PbBr_2$, the authors hypothesized that similar defects are responsible for these two processes. These defects may result from undercoordinated lead atoms that cause shallow trap states close in energy to the band edges and whose density decreases with the addition of a bromide source. In order for $CsPbBr_3$ nanoplatelets to reach near-unity PLQYs, however, chemical treatments that address the significant dark fraction of nanoplatelets still must be developed.

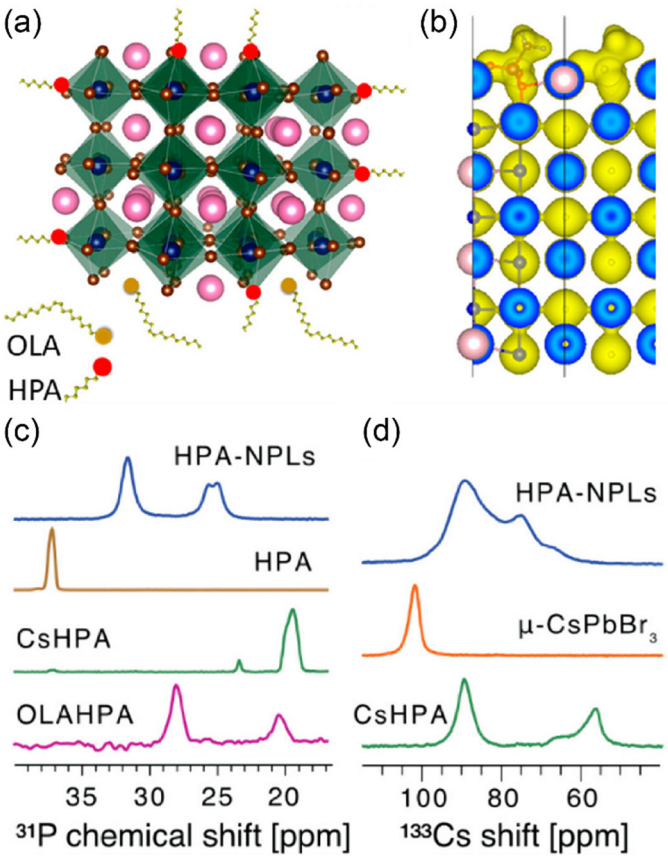

Figure 10. (a) DFT calculated structure of a $CsPbBr_3$ nanoplatelet coordinated by oleylammonium (OLA) and hexylphosphonate (HPA) ligands. Cs, Pb, and Br atoms are denoted by pink, blue, and brown spheres, respectively. (b) Total electron density (denoted as yellow isosurfaces) of the nanoplatelets passivated with methylamine and methylphosphonate ligands. (c) ^{1}H–^{31}P CP MAS NMR spectra of HPA-capped $CsPbBr_3$ nanoplatelets, neat HPA, cesium hexylphoshonate (CsHPA), and oleylammonium hexylphosphonate (OLAHPA). (d) ^{133}Cs MAS NMR spectra of HPA-capped $CsPbBr_3$ nanoplatelets, microcrystalline $CsPbBr_3$ (μ-$CsPbBr_3$), and CsHPA. Reproduced with permission from ref. 90. Copyright (2020) American Chemical Society.

Stranks and co-workers reported the addition of hexylphosphonic acid to 4-ML thick $CsPbBr_3$ nanoplatelets synthesized with oleic acid and oleylamine. The PLQY of the $CsPbBr_3$ nanoplatelets increased from ~25% to ~40% upon addition of hexylphosphonic acid during synthesis. DFT calculations predicted strong binding of a model alkylphosphonate ligand (methylphosphonate) on the {100} facet of a CsBr-terminated $CsPbBr_3$ nanoplatelet (**Figure 10a,b**). The ^{1}H-^{31}P CP MAS solid-state NMR spectrum of the hexylphosphonate-ligated $CsPbBr_3$ nanoplatelets gave a complex mixture of four resonances (31.6, 29.8, 25.7, and 24.9 ppm) that

were assigned to different binding sites on the nanoplatelet surface (**Figure 10c**). These sites differ from those observed for cuboidal $CsPbBr_3$ nanocrystals (*vide supra*). The ^{133}Cs MAS NMR spectrum of the hexylphosphonate-ligated $CsPbBr_3$ nanoplatelets gave a broad set of resonances spanning from 60-100 ppm (**Figure 10d**). The major resonance at ca. 100 ppm is consistent with a "bulk-like" cesium environment of microcrystals and cuboidal nanocrystals of $CsPbBr_3$.[4,91,92] The nanoplatelets possess a second major peak at ca. 75 ppm, well upfield of the reported chemical shift of 170 ppm for surface Cs in 10-undecenylphosphonic- and oleic acid-capped cuboidal $CsPbBr_3$ nanocrystals. Further solid-state NMR experiments are required to conclusively assign the ^{133}Cs signals to different Cs environments in the cuboids and nanoplatelets and explain the large differences in ^{133}Cs chemical shifts.

5. CONCLUSIONS AND OUTLOOK

In this Account, we reviewed the current state-of-the-art with respect to knowledge about the surface chemistry of the most studied lead halide perovskite nanocrystal composition of $CsPbBr_3$. We focused on the foundational work that has been done to better understand the native surface chemistry of $CsPbBr_3$ nanocrystals and post-synthetic surface treatments used to minimize their surface trap-state density and improve PLQY. While much of the surface chemistry specific to $CsPbBr_3$ nanocrystals should be generally applicable to the whole family of lead halide perovskite nanocrystals with other A-site cations, such as MA and formamidinium, the surface chemistry of these compositional derivates is under studied.

The surface chemistry of lead halide perovskite nanocrystals is unique due to their highly ionic structure, which causes chemical instability and somewhat limits surface passivation options; however, the work described above leverages what is known about the surface structure of these

nanocrystals to improve passivation with tighter binding ligands and/or heal surface defects. Despite the success of the post-synthetic treatments, a clear experimental understanding of the mechanisms of ligand binding, surface reconstruction, and trap-state healing remain unexplored. It will be critical to develop a detailed experimental understanding of how the surface chemistry of these nanocrystals change after treatment with ligands. With a greater understanding of the ensuing surface structure upon post-synthetic ligand treatments, next-generation ligand design may enable further improvements in the properties of these nanocrystals. For example, it remains to be seen whether the permanently dark fraction of $CsPbBr_3$ nanocrystals may be addressed by judicious choice of surface treatment. Post-synthetic surface treatments that facilitate improved exciton management in lead halide perovskite nanocrystals and improve their stability will be critical for the commercial adoption of these materials. Upon moving from nanocrystals to microcrystals, it is possible that different types of surfaces and defects may be encountered. However, the knowledge gained from the study of nanocrystal surface chemistry should provide a framework to develop passivation strategies for polycrystalline lead halide perovskite thin films.

AUTHOR INFORMATION

Corresponding Author

*E-mail: brutchey@usc.edu

*E-mail: arossini@iastate.edu

Author Contributions

†S.R.S. and Y.C. contributed equally to this work.

Biography

Sara R. Smock is a National Science Foundation Graduate Research Fellow and Ph.D. candidate under the supervision of Prof. Brutchey at the University of Southern California. Her research focuses on the study of surfaces and ligand exchange reactions of quantum dots.

Yunhua Chen is a Ph.D. candidate under the supervision of Professors Rossini and Vela at Iowa State University. Her research focuses on the development and application of solid-state NMR spectroscopy for surface characterization of semiconductor nanomaterials.

Aaron J. Rossini is an Assistant Professor of Chemistry at Iowa State University and is also affiliated with the US DOE Ames Laboratory. The Rossini group develops solid-state NMR spectroscopy for the structural characterization of materials. He was named a 2020 Alfred P Sloan Research Fellow.

Richard L. Brutchey is a Professor of Chemistry at the University of Southern California. The Brutchey group focuses on the design of inorganic materials to address challenges in catalysis, energy conversion, and sustainability. His honors include being named a 2010 Cottrell Scholar and receiving the 2020 ACS Nanoscience Award.

ACKNOWLEDGMENT

R.L.B. acknowledges financial support by the U.S. Department of Energy, Office of Science, Basic Energy Sciences, under Award DE-FG02-11ER46826. S.R.S. acknowledges support from the Graduate Research Fellowship Program of the National Science Foundation. A.J.R. and Y.C. were supported by the U.S. Department of Energy (DOE), Office of Science, Basic Energy Sciences, Materials Science and Engineering Division. The Ames Laboratory is operated for the U.S. DOE

by Iowa State University under contract # DE-AC02-07CH11358. A.J.R. acknowledges additional support from the Alfred P. Sloan Foundation through a Sloan research fellowship.

REFERENCES

(1) Cottingham, P.; Brutchey, R. L. On the Crystal Structure of Colloidally Prepared $CsPbBr_3$ Quantum Dots. *Chem. Commun.* **2016**, *52* (30), 5246–5249. https://doi.org/10.1039/C6CC01088A.

(2) Hanrahan, M. P.; Men, L.; Rosales, B. A.; Vela, J.; Rossini, A. J. Sensitivity-Enhanced ^{207} Pb Solid-State NMR Spectroscopy for the Rapid, Non-Destructive Characterization of Organolead Halide Perovskites. *Chem. Mater.* **2018**, *30* (20), 7005–7015. https://doi.org/10.1021/acs.chemmater.8b01899.

(3) Smock, S. R.; Williams, T. J.; Brutchey, R. L. Quantifying the Thermodynamics of Ligand Binding to $CsPbBr_3$ Quantum Dots. *Angew. Chem. Int. Ed.* **2018**, *57* (36), 11711–11715. https://doi.org/10.1002/anie.201806916.

(4) Chen, Y.; Smock, S. R.; Flintgruber, A. H.; Perras, F. A.; Brutchey, R. L.; Rossini, A. J. Surface Termination of $CsPbBr_3$ Perovskite Quantum Dots Determined by Solid-State NMR Spectroscopy. *J. Am. Chem. Soc.* **2020**, *142* (13), 6117–6127. https://doi.org/10.1021/jacs.9b13396.

(5) Rose, G. Ueber einige neue Mineralien des Urals. *J. Prakt. Chem.* **1840**, *19* (1), 459–468. https://doi.org/10.1002/prac.18400190179.

(6) Bhalla, A. S.; Guo, R.; Roy, R. The Perovskite Structure—a Review of Its Role in Ceramic Science and Technology. *Mater. Res. Innov.* **2000**, *4* (1), 3–26. https://doi.org/10.1007/s100190000062.

(7) Breternitz, J.; Schorr, S. What Defines a Perovskite? *Adv. Energy Mater.* **2018**, *8* (34), 1802366. https://doi.org/10.1002/aenm.201802366.

(8) Niu, S.; Huyan, H.; Liu, Y.; Yeung, M.; Ye, K.; Blankemeier, L.; Orvis, T.; Sarkar, D.; Singh, D. J.; Kapadia, R.; Ravichandran, J. Bandgap Control via Structural and Chemical Tuning of Transition Metal Perovskite Chalcogenides. *Adv. Mater.* **2017**, *29* (9), 1604733. https://doi.org/10.1002/adma.201604733.

(9) Talley, K. R.; Perkins, C. L.; Diercks, D. R.; Brennecka, G. L.; Zakutayev, A. Synthesis of Ferroelectric LaWN3 -- the First Nitride Perovskite. *arXiv:2001.00633 [cond-mat]* **2020**.

(10) Stoumpos, C. C.; Malliakas, C. D.; Peters, J. A.; Liu, Z.; Sebastian, M.; Im, J.; Chasapis, T. C.; Wibowo, A. C.; Chung, D. Y.; Freeman, A. J.; Wessels, B. W.; Kanatzidis, M. G. Crystal Growth of the Perovskite Semiconductor $CsPbBr_3$: A New Material for High-Energy Radiation Detection. *Cryst. Growth Des.* **2013**, *13* (7), 2722–2727. https://doi.org/10.1021/cg400645t.

(11) Wells, H. L. Über Die Cäsium- Und Kalium-Bleihalogenide. *Z. Anorg. Chem.* **1893**, *3* (1), 195–210. https://doi.org/10.1002/zaac.18930030124.

(12) Best Research-Cell Efficiencies https://www.nrel.gov/pv/assets/pdfs/best-research-cell-efficiencies.20200708.pdf (accessed Jul 30, 2020).

(13) Noel, N. K.; Abate, A.; Stranks, S. D.; Parrott, E. S.; Burlakov, V. M.; Goriely, A.; Snaith, H. J. Enhanced Photoluminescence and Solar Cell Performance *via* Lewis Base Passivation

of Organic–Inorganic Lead Halide Perovskites. *ACS Nano* **2014**, *8* (10), 9815–9821. https://doi.org/10.1021/nn5036476.

(14) deQuilettes, D. W.; Koch, S.; Burke, S.; Paranji, R. K.; Shropshire, A. J.; Ziffer, M. E.; Ginger, D. S. Photoluminescence Lifetimes Exceeding 8 Ms and Quantum Yields Exceeding 30% in Hybrid Perovskite Thin Films by Ligand Passivation. *ACS Energy Lett.* **2016**, *1* (2), 438–444. https://doi.org/10.1021/acsenergylett.6b00236.

(15) Hawash, Z.; Raga, S. R.; Son, D.-Y.; Ono, L. K.; Park, N.-G.; Qi, Y. Interfacial Modification of Perovskite Solar Cells Using an Ultrathin MAI Layer Leads to Enhanced Energy Level Alignment, Efficiencies, and Reproducibility. *J. Phys. Chem. Lett.* **2017**, *8* (17), 3947–3953. https://doi.org/10.1021/acs.jpclett.7b01508.

(16) Alharbi, E. A.; Alyamani, A. Y.; Kubicki, D. J.; Uhl, A. R.; Walder, B. J.; Alanazi, A. Q.; Luo, J.; Burgos-Caminal, A.; Albadri, A.; Albrithen, H.; Alotaibi, M. H.; Moser, J.-E.; Zakeeruddin, S. M.; Giordano, F.; Emsley, L.; Grätzel, M. Atomic-Level Passivation Mechanism of Ammonium Salts Enabling Highly Efficient Perovskite Solar Cells. *Nat. Commun* **2019**, *10* (1), 3008. https://doi.org/10.1038/s41467-019-10985-5.

(17) Hewavitharana, I. K.; Brock, S. L. When Ligand Exchange Leads to Ion Exchange: Nanocrystal Facets Dictate the Outcome. *ACS Nano* **2017**, *11* (11), 11217–11224. https://doi.org/10.1021/acsnano.7b05534.

(18) Choi, H.; Kim, S.; Luther, J. M.; Kim, S.-W.; Shin, D.; Beard, M. C.; Jeong, S. Facet-Specific Ligand Interactions on Ternary $AgSbS_2$ Colloidal Quantum Dots. *Chem. Eur. J.* **2017**, *23* (70), 17707–17713. https://doi.org/10.1002/chem.201703681.

(19) Morris-Cohen, A. J.; Frederick, M. T.; Lilly, G. D.; McArthur, E. A.; Weiss, E. A. Organic Surfactant-Controlled Composition of the Surfaces of CdSe Quantum Dots. *J. Phys. Chem. Lett.* **2010**, *1* (7), 1078–1081. https://doi.org/10.1021/jz100224q.

(20) Moreels, I.; Lambert, K.; De Muynck, D.; Vanhaecke, F.; Poelman, D.; Martins, J. C.; Allan, G.; Hens, Z. Composition and Size-Dependent Extinction Coefficient of Colloidal PbSe Quantum Dots. *Chem. Mater.* **2007**, *19* (25), 6101–6106. https://doi.org/10.1021/cm071410q.

(21) Bullen, C.; Mulvaney, P. The Effects of Chemisorption on the Luminescence of CdSe Quantum Dots. *Langmuir* **2006**, *22* (7), 3007–3013. https://doi.org/10.1021/la051898e.

(22) Buckley, J. J.; Couderc, E.; Greaney, M. J.; Munteanu, J.; Riche, C. T.; Bradforth, S. E.; Brutchey, R. L. Chalcogenol Ligand Toolbox for CdSe Nanocrystals and Their Influence on Exciton Relaxation Pathways. *ACS Nano* **2014**, *8* (3), 2512–2521. https://doi.org/10.1021/nn406109v.

(23) Frederick, M. T.; Weiss, E. A. Relaxation of Exciton Confinement in CdSe Quantum Dots by Modification with a Conjugated Dithiocarbamate Ligand. *ACS Nano* **2010**, *4* (6), 3195–3200. https://doi.org/10.1021/nn1007435.

(24) Grigel, V.; Sagar, L. K.; De Nolf, K.; Zhao, Q.; Vantomme, A.; De Roo, J.; Infante, I.; Hens, Z. The Surface Chemistry of Colloidal HgSe Nanocrystals, toward Stoichiometric Quantum Dots by Design. *Chem. Mater.* **2018**, *30* (21), 7637–7647. https://doi.org/10.1021/acs.chemmater.8b02908.

(25) Smock, S. R.; Tabatabaei, K.; Williams, T. J.; Kauzlarich, S. M.; Brutchey, R. L. Surface Coordination Chemistry of Germanium Nanocrystals Synthesized by Microwave-Assisted Reduction in Oleylamine. *Nanoscale* **2020**, *12* (4), 2764–2772. https://doi.org/10.1039/C9NR09233A.

(26) Wheeler, L. M.; Nichols, A. W.; Chernomordik, B. D.; Anderson, N. C.; Beard, M. C.; Neale, N. R. All-Inorganic Germanium Nanocrystal Films by Cationic Ligand Exchange. *Nano Lett.* **2016**, *16* (3), 1949–1954. https://doi.org/10.1021/acs.nanolett.5b05192.
(27) Sandeep, K.; Gopika, K. Y.; Revathi, M. R. Role of Capped Oleyl Amine in the Moisture-Induced Structural Transformation of $CsPbBr_3$ Perovskite Nanocrystals. *Phys. Status Solidi RRL* **2019**, *13* (11), 1900387. https://doi.org/10.1002/pssr.201900387.
(28) ten Brinck, S.; Infante, I. Surface Termination, Morphology, and Bright Photoluminescence of Cesium Lead Halide Perovskite Nanocrystals. *ACS Energy Lett.* **2016**, *1* (6), 1266–1272. https://doi.org/10.1021/acsenergylett.6b00595.
(29) De Roo, J.; Ibáñez, M.; Geiregat, P.; Nedelcu, G.; Walravens, W.; Maes, J.; Martins, J. C.; Van Driessche, I.; Kovalenko, M. V.; Hens, Z. Highly Dynamic Ligand Binding and Light Absorption Coefficient of Cesium Lead Bromide Perovskite Nanocrystals. *ACS Nano* **2016**, *10* (2), 2071–2081. https://doi.org/10.1021/acsnano.5b06295.
(30) Kovalenko, M. V.; Protesescu, L.; Bodnarchuk, M. I. Properties and Potential Optoelectronic Applications of Lead Halide Perovskite Nanocrystals. *Science* **2017**, *358* (6364), 745–750. https://doi.org/10.1126/science.aam7093.
(31) Huang, H.; Bodnarchuk, M. I.; Kershaw, S. V.; Kovalenko, M. V.; Rogach, A. L. Lead Halide Perovskite Nanocrystals in the Research Spotlight: Stability and Defect Tolerance. *ACS Energy Lett.* **2017**, *2* (9), 2071–2083. https://doi.org/10.1021/acsenergylett.7b00547.
(32) Yan, F.; Tan, S. T.; Li, X.; Demir, H. V. Light Generation in Lead Halide Perovskite Nanocrystals: LEDs, Color Converters, Lasers, and Other Applications. *Small* **2019**, *15* (47), 1902079. https://doi.org/10.1002/smll.201902079.
(33) Schmidt, L. C.; Pertegás, A.; González-Carrero, S.; Malinkiewicz, O.; Agouram, S.; Mínguez Espallargas, G.; Bolink, H. J.; Galian, R. E.; Pérez-Prieto, J. Nontemplate Synthesis of $CH_3NH_3PbBr_3$ Perovskite Nanoparticles. *J. Am. Chem. Soc.* **2014**, *136* (3), 850–853. https://doi.org/10.1021/ja4109209.
(34) Wei, S.; Yang, Y.; Kang, X.; Wang, L.; Huang, L.; Pan, D. Room-Temperature and Gram-Scale Synthesis of $CsPbX_3$ (X = Cl, Br, I) Perovskite Nanocrystals with 50–85% Photoluminescence Quantum Yields. *Chem. Commun.* **2016**, *52* (45), 7265–7268. https://doi.org/10.1039/C6CC01500J.
(35) Protesescu, L.; Yakunin, S.; Bodnarchuk, M. I.; Krieg, F.; Caputo, R.; Hendon, C. H.; Yang, R. X.; Walsh, A.; Kovalenko, M. V. Nanocrystals of Cesium Lead Halide Perovskites (CsPbX3, X = Cl, Br, and I): Novel Optoelectronic Materials Showing Bright Emission with Wide Color Gamut. *Nano Lett.* **2015**, *15* (6), 3692–3696. https://doi.org/10.1021/nl5048779.
(36) Cottingham, P.; Brutchey, R. L. Compositionally Dependent Phase Identity of Colloidal $CsPbBr_{3-x}I_x$ Quantum Dots. *Chem. Commun.* **2016**, *28* (21), 7574–7577. https://doi.org/10.1021/acs.chemmater.6b03553.
(37) Cottingham, P.; Brutchey, R. L. Depressed Phase Transitions and Thermally Persistent Local Distortions in $CsPbBr_3$ Quantum Dots. *Chem. Mater.* **2018**, *30* (19), 6711–6716. https://doi.org/10.1021/acs.chemmater.8b02295.
(38) Pan, A.; He, B.; Fan, X.; Liu, Z.; Urban, J. J.; Alivisatos, A. P.; He, L.; Liu, Y. Insight into the Ligand-Mediated Synthesis of Colloidal $CsPbBr_3$ Perovskite Nanocrystals: The Role of Organic Acid, Base, and Cesium Precursors. *ACS Nano* **2016**, *10* (8), 7943–7954. https://doi.org/10.1021/acsnano.6b03863.

(39) Brennan, M. C.; Kuno, M.; Rouvimov, S. Crystal Structure of Individual $CsPbBr_3$ Perovskite Nanocubes. *Inorg. Chem.* **2019**, *58* (2), 1555–1560. https://doi.org/10.1021/acs.inorgchem.8b03078.

(40) Ravi, V. K.; Santra, P. K.; Joshi, N.; Chugh, J.; Singh, S. K.; Rensmo, H.; Ghosh, P.; Nag, A. Origin of the Substitution Mechanism for the Binding of Organic Ligands on the Surface of $CsPbBr_3$ Perovskite Nanocubes. *J. Phys. Chem. Lett.* **2017**, *8* (20), 4988–4994. https://doi.org/10.1021/acs.jpclett.7b02192.

(41) Bodnarchuk, M. I.; Boehme, S. C.; ten Brinck, S.; Bernasconi, C.; Shynkarenko, Y.; Krieg, F.; Widmer, R.; Aeschlimann, B.; Günther, D.; Kovalenko, M. V.; Infante, I. Rationalizing and Controlling the Surface Structure and Electronic Passivation of Cesium Lead Halide Nanocrystals. *ACS Energy Lett.* **2019**, *4* (1), 63–74. https://doi.org/10.1021/acsenergylett.8b01669.

(42) Stoumpos, C. C.; Cao, D. H.; Clark, D. J.; Young, J.; Rondinelli, J. M.; Jang, J. I.; Hupp, J. T.; Kanatzidis, M. G. Ruddlesden–Popper Hybrid Lead Iodide Perovskite 2D Homologous Semiconductors. *Chem. Mater.* **2016**, *28* (8), 2852–2867. https://doi.org/10.1021/acs.chemmater.6b00847.

(43) Tong, Y.; Bladt, E.; Aygüler, M. F.; Manzi, A.; Milowska, K. Z.; Hintermayr, V. A.; Docampo, P.; Bals, S.; Urban, A. S.; Polavarapu, L.; Feldmann, J. Highly Luminescent Cesium Lead Halide Perovskite Nanocrystals with Tunable Composition and Thickness by Ultrasonication. *Angew. Chem. Int. Ed.* **2016**, *55* (44), 13887–13892. https://doi.org/10.1002/anie.201605909.

(44) Bertolotti, F.; Protesescu, L.; Kovalenko, M. V.; Yakunin, S.; Cervellino, A.; Billinge, S. J. L.; Terban, M. W.; Pedersen, J. S.; Masciocchi, N.; Guagliardi, A. Coherent Nanotwins and Dynamic Disorder in Cesium Lead Halide Perovskite Nanocrystals. *ACS Nano* **2017**, *11* (4), 3819–3831. https://doi.org/10.1021/acsnano.7b00017.

(45) Antanovich, A.; Prudnikau, A.; Matsukovich, A.; Achtstein, A.; Artemyev, M. Self-Assembly of CdSe Nanoplatelets into Stacks of Controlled Size Induced by Ligand Exchange. *J. Phys. Chem. C* **2016**, *120* (10), 5764–5775. https://doi.org/10.1021/acs.jpcc.5b12139.

(46) Wang, S.; Du, L.; Jin, Z.; Xin, Y.; Mattoussi, H. Enhanced Stabilization and Easy Phase Transfer of $CsPbBr_3$ Perovskite Quantum Dots Promoted by High-Affinity Polyzwitterionic Ligands. *J. Am. Chem. Soc.* **2020**, *142* (29), 12669–12680. https://doi.org/10.1021/jacs.0c03682.

(47) Quarta, D.; Imran, M.; Capodilupo, A.-L.; Petralanda, U.; van Beek, B.; De Angelis, F.; Manna, L.; Infante, I.; De Trizio, L.; Giansante, C. Stable Ligand Coordination at the Surface of Colloidal $CsPbBr_3$ Nanocrystals. *J. Phys. Chem. Lett.* **2019**, *10* (13), 3715–3726. https://doi.org/10.1021/acs.jpclett.9b01634.

(48) Imran, M.; Ijaz, P.; Goldoni, L.; Maggioni, D.; Petralanda, U.; Prato, M.; Almeida, G.; Infante, I.; Manna, L. Simultaneous Cationic and Anionic Ligand Exchange For Colloidally Stable $CsPbBr_3$ Nanocrystals. *ACS Energy Lett.* **2019**, *4* (4), 819–824. https://doi.org/10.1021/acsenergylett.9b00140.

(49) Ijaz, P.; Imran, M.; Soares, M. M.; Tolentino, H. C. N.; Martín-García, B.; Giannini, C.; Moreels, I.; Manna, L.; Krahne, R. Composition-, Size-, and Surface Functionalization-Dependent Optical Properties of Lead Bromide Perovskite Nanocrystals. *J. Phys. Chem. Lett.* **2020**, *11* (6), 2079–2085. https://doi.org/10.1021/acs.jpclett.0c00266.

(50) Krieg, F.; Ochsenbein, S. T.; Yakunin, S.; ten Brinck, S.; Aellen, P.; Süess, A.; Clerc, B.; Guggisberg, D.; Nazarenko, O.; Shynkarenko, Y.; Kumar, S.; Shih, C.-J.; Infante, I.; Kovalenko, M. V. Colloidal $CsPbX_3$ (X = Cl, Br, I) Nanocrystals 2.0: Zwitterionic Capping Ligands for Improved Durability and Stability. *ACS Energy Lett.* **2018**, *3* (3), 641–646. https://doi.org/10.1021/acsenergylett.8b00035.

(51) Schwarzenbach, G. Der Chelateffekt. *Helv. Chim. Acta* **1952**, *35* (7), 2344–2359. https://doi.org/10.1002/hlca.19520350721.

(52) Krieg, F.; Ong, Q. K.; Burian, M.; Rainò, G.; Naumenko, D.; Amenitsch, H.; Süess, A.; Grotevent, M. J.; Krumeich, F.; Bodnarchuk, M. I.; Shorubalko, I.; Stellacci, F.; Kovalenko, M. V. Stable Ultraconcentrated and Ultradilute Colloids of $CsPbX_3$ (X = Cl, Br) Nanocrystals Using Natural Lecithin as a Capping Ligand. *J. Am. Chem. Soc.* **2019**, *141* (50), 19839–19849. https://doi.org/10.1021/jacs.9b09969.

(53) De Gennes, P. G. Polymer Solutions near an Interface. Adsorption and Depletion Layers. *Macromolecules* **1981**, *14* (6), 1637–1644. https://doi.org/10.1021/ma50007a007.

(54) De Gennes, P. G. Polymers at an Interface. 2. Interaction between Two Plates Carrying Adsorbed Polymer Layers. *Macromolecules* **1982**, *15* (2), 492–500. https://doi.org/10.1021/ma00230a055.

(55) De Gennes, P. G. Polymers at an Interface; a Simplified View. *Adv. Colloid Interface Sci.* **1987**, *27* (3–4), 189–209. https://doi.org/10.1016/0001-8686(87)85003-0.

(56) Tan, Y.; Zou, Y.; Wu, L.; Huang, Q.; Yang, D.; Chen, M.; Ban, M.; Wu, C.; Wu, T.; Bai, S.; Song, T.; Zhang, Q.; Sun, B. Highly Luminescent and Stable Perovskite Nanocrystals with Octylphosphonic Acid as a Ligand for Efficient Light-Emitting Diodes. *ACS Appl. Mater. Interfaces* **2018**, *10* (4), 3784–3792. https://doi.org/10.1021/acsami.7b17166.

(57) Koh, W.; Park, S.; Ham, Y. Phosphonic Acid Stabilized Colloidal $CsPbX_3$ (X=Br, I) Perovskite Nanocrystals and Their Surface Chemistry. *ChemistrySelect* **2016**, *1* (13), 3479–3482. https://doi.org/10.1002/slct.201600809.

(58) Nenon, D. P.; Pressler, K.; Kang, J.; Koscher, B. A.; Olshansky, J. H.; Osowiecki, W. T.; Koc, M. A.; Wang, L.-W.; Alivisatos, A. P. Design Principles for Trap-Free $CsPbX_3$ Nanocrystals: Enumerating and Eliminating Surface Halide Vacancies with Softer Lewis Bases. *J. Am. Chem. Soc.* **2018**, *140* (50), 17760–17772. https://doi.org/10.1021/jacs.8b11035.

(59) Brown, A. A. M.; Hooper, T. J. N.; Veldhuis, S. A.; Chin, X. Y.; Bruno, A.; Vashishtha, P.; Tey, J. N.; Jiang, L.; Damodaran, B.; Pu, S. H.; Mhaisalkar, S. G.; Mathews, N. Self-Assembly of a Robust Hydrogen-Bonded Octylphosphonate Network on Cesium Lead Bromide Perovskite Nanocrystals for Light-Emitting Diodes. *Nanoscale* **2019**, *11* (25), 12370–12380. https://doi.org/10.1039/C9NR02566A.

(60) Yang, D.; Li, X.; Zhou, W.; Zhang, S.; Meng, C.; Wu, Y.; Wang, Y.; Zeng, H. $CsPbBr_3$ Quantum Dots 2.0: Benzenesulfonic Acid Equivalent Ligand Awakens Complete Purification. *Adv. Mater.* **2019**, 1900767. https://doi.org/10.1002/adma.201900767.

(61) Kovalenko, M. V.; Scheele, M.; Talapin, D. V. Colloidal Nanocrystals with Molecular Metal Chalcogenide Surface Ligands. *Science* **2009**, *324* (5933), 1417–1420. https://doi.org/10.1126/science.1170524.

(62) Wang, Y.; Fedin, I.; Zhang, H.; Talapin, D. V. Direct Optical Lithography of Functional Inorganic Nanomaterials. *Science* **2017**, *357* (6349), 385–388. https://doi.org/10.1126/science.aan2958.

(63) Webber, D. H.; Brutchey, R. L. Ligand Exchange on Colloidal CdSe Nanocrystals Using Thermally Labile *Tert* -Butylthiol for Improved Photocurrent in Nanocrystal Films. *J. Am. Chem. Soc.* **2012**, *134* (2), 1085–1092. https://doi.org/10.1021/ja208878h.

(64) Pan, J.; Quan, L. N.; Zhao, Y.; Peng, W.; Murali, B.; Sarmah, S. P.; Yuan, M.; Sinatra, L.; Alyami, N. M.; Liu, J.; Yassitepe, E.; Yang, Z.; Voznyy, O.; Comin, R.; Hedhili, M. N.; Mohammed, O. F.; Lu, Z. H.; Kim, D. H.; Sargent, E. H.; Bakr, O. M. Highly Efficient Perovskite-Quantum-Dot Light-Emitting Diodes by Surface Engineering. *Adv. Mater.* **2016**, *28* (39), 8718–8725. https://doi.org/10.1002/adma.201600784.

(65) Song, J.; Li, J.; Li, X.; Xu, L.; Dong, Y.; Zeng, H. Quantum Dot Light-Emitting Diodes Based on Inorganic Perovskite Cesium Lead Halides ($CsPbX_3$). *Adv. Mater.* **2015**, *27* (44), 7162–7167. https://doi.org/10.1002/adma.201502567.

(66) Dong, Y.; Wang, Y.-K.; Yuan, F.; Johnston, A.; Liu, Y.; Ma, D.; Choi, M.-J.; Chen, B.; Chekini, M.; Baek, S.-W.; Sagar, L. K.; Fan, J.; Hou, Y.; Wu, M.; Lee, S.; Sun, B.; Hoogland, S.; Quintero-Bermudez, R.; Ebe, H.; Todorovic, P.; Dinic, F.; Li, P.; Kung, H. T.; Saidaminov, M. I.; Kumacheva, E.; Spiecker, E.; Liao, L.-S.; Voznyy, O.; Lu, Z.-H.; Sargent, E. H. Bipolar-Shell Resurfacing for Blue LEDs Based on Strongly Confined Perovskite Quantum Dots. *Nat. Nanotechnol.* **2020**, *15* (8), 668–674. https://doi.org/10.1038/s41565-020-0714-5.

(67) Wheeler, L. M.; Sanehira, E. M.; Marshall, A. R.; Schulz, P.; Suri, M.; Anderson, N. C.; Christians, J. A.; Nordlund, D.; Sokaras, D.; Kroll, T.; Harvey, S. P.; Berry, J. J.; Lin, L. Y.; Luther, J. M. Targeted Ligand-Exchange Chemistry on Cesium Lead Halide Perovskite Quantum Dots for High-Efficiency Photovoltaics. *J. Am. Chem. Soc.* **2018**, *140* (33), 10504–10513. https://doi.org/10.1021/jacs.8b04984.

(68) Wang, Y.; Yuan, J.; Zhang, X.; Ling, X.; Larson, B. W.; Zhao, Q.; Yang, Y.; Shi, Y.; Luther, J. M.; Ma, W. Surface Ligand Management Aided by a Secondary Amine Enables Increased Synthesis Yield of $CsPbI_3$ Perovskite Quantum Dots and High Photovoltaic Performance. *Adv. Mater.* **2020**, *32* (32), 2000449. https://doi.org/10.1002/adma.202000449.

(69) Zhang, D.; Eaton, S. W.; Yu, Y.; Dou, L.; Yang, P. Solution-Phase Synthesis of Cesium Lead Halide Perovskite Nanowires. *J. Am. Chem. Soc.* **2015**, *137* (29), 9230–9233. https://doi.org/10.1021/jacs.5b05404.

(70) Imran, M.; Di Stasio, F.; Dang, Z.; Canale, C.; Khan, A. H.; Shamsi, J.; Brescia, R.; Prato, M.; Manna, L. Colloidal Synthesis of Strongly Fluorescent $CsPbBr_3$ Nanowires with Width Tunable down to the Quantum Confinement Regime. *Chem. Mater.* **2016**, *28* (18), 6450–6454. https://doi.org/10.1021/acs.chemmater.6b03081.

(71) Zhang, D.; Yu, Y.; Bekenstein, Y.; Wong, A. B.; Alivisatos, A. P.; Yang, P. Ultrathin Colloidal Cesium Lead Halide Perovskite Nanowires. *J. Am. Chem. Soc.* **2016**, *138* (40), 13155–13158. https://doi.org/10.1021/jacs.6b08373.

(72) Liu, J.; Song, K.; Shin, Y.; Liu, X.; Chen, J.; Yao, K. X.; Pan, J.; Yang, C.; Yin, J.; Xu, L.-J.; Yang, H.; El-Zohry, A. M.; Xin, B.; Mitra, S.; Hedhili, M. N.; Roqan, I. S.; Mohammed, O. F.; Han, Y.; Bakr, O. M. Light-Induced Self-Assembly of Cubic $CsPbBr_3$ Perovskite Nanocrystals into Nanowires. *Chem. Mater.* **2019**, *31* (17), 6642–6649. https://doi.org/10.1021/acs.chemmater.9b00680.

(73) Akkerman, Q. A.; Motti, S. G.; Srimath Kandada, A. R.; Mosconi, E.; D'Innocenzo, V.; Bertoni, G.; Marras, S.; Kamino, B. A.; Miranda, L.; De Angelis, F.; Petrozza, A.; Prato, M.; Manna, L. Solution Synthesis Approach to Colloidal Cesium Lead Halide Perovskite

Nanoplatelets with Monolayer-Level Thickness Control. *J. Am. Chem. Soc.* **2016**, *138* (3), 1010–1016. https://doi.org/10.1021/jacs.5b12124.

(74) Li, J.; Luo, L.; Huang, H.; Ma, C.; Ye, Z.; Zeng, J.; He, H. 2D Behaviors of Excitons in Cesium Lead Halide Perovskite Nanoplatelets. *J. Phys. Chem. Lett.* **2017**, *8* (6), 1161–1168. https://doi.org/10.1021/acs.jpclett.7b00017.

(75) Bohn, B. J.; Tong, Y.; Gramlich, M.; Lai, M. L.; Döblinger, M.; Wang, K.; Hoye, R. L. Z.; Müller-Buschbaum, P.; Stranks, S. D.; Urban, A. S.; Polavarapu, L.; Feldmann, J. Boosting Tunable Blue Luminescence of Halide Perovskite Nanoplatelets through Postsynthetic Surface Trap Repair. *Nano Lett.* **2018**, *18* (8), 5231–5238. https://doi.org/10.1021/acs.nanolett.8b02190.

(76) Isarov, M.; Tan, L. Z.; Bodnarchuk, M. I.; Kovalenko, M. V.; Rappe, A. M.; Lifshitz, E. Rashba Effect in a Single Colloidal $CsPbBr_3$ Perovskite Nanocrystal Detected by Magneto-Optical Measurements. *Nano Lett.* **2017**, *17* (8), 5020–5026. https://doi.org/10.1021/acs.nanolett.7b02248.

(77) Hintermayr, V. A.; Polavarapu, L.; Urban, A. S.; Feldmann, J. Accelerated Carrier Relaxation through Reduced Coulomb Screening in Two-Dimensional Halide Perovskite Nanoplatelets. *ACS Nano* **2018**, *12* (10), 10151–10158. https://doi.org/10.1021/acsnano.8b05029.

(78) Ling, Y.; Yuan, Z.; Tian, Y.; Wang, X.; Wang, J. C.; Xin, Y.; Hanson, K.; Ma, B.; Gao, H. Bright Light-Emitting Diodes Based on Organometal Halide Perovskite Nanoplatelets. *Adv. Mater.* **2016**, *28* (2), 305–311. https://doi.org/10.1002/adma.201503954.

(79) Xing, J.; Zhao, Y.; Askerka, M.; Quan, L. N.; Gong, X.; Zhao, W.; Zhao, J.; Tan, H.; Long, G.; Gao, L.; Yang, Z.; Voznyy, O.; Tang, J.; Lu, Z.-H.; Xiong, Q.; Sargent, E. H. Color-Stable Highly Luminescent Sky-Blue Perovskite Light-Emitting Diodes. *Nat. Commun* **2018**, *9* (1), 3541. https://doi.org/10.1038/s41467-018-05909-8.

(80) Hoye, R. L. Z.; Lai, M.-L.; Anaya, M.; Tong, Y.; Gałkowski, K.; Doherty, T.; Li, W.; Huq, T. N.; Mackowski, S.; Polavarapu, L.; Feldmann, J.; MacManus-Driscoll, J. L.; Friend, R. H.; Urban, A. S.; Stranks, S. D. Identifying and Reducing Interfacial Losses to Enhance Color-Pure Electroluminescence in Blue-Emitting Perovskite Nanoplatelet Light-Emitting Diodes. *ACS Energy Lett.* **2019**, *4* (5), 1181–1188. https://doi.org/10.1021/acsenergylett.9b00571.

(81) Bertolotti, F.; Nedelcu, G.; Vivani, A.; Cervellino, A.; Masciocchi, N.; Guagliardi, A.; Kovalenko, M. V. Crystal Structure, Morphology, and Surface Termination of Cyan-Emissive, Six-Monolayers-Thick $CsPbBr_3$ Nanoplatelets from X-Ray Total Scattering. *ACS Nano* **2019**, *13* (12), 14294–14307. https://doi.org/10.1021/acsnano.9b07626.

(82) Bekenstein, Y.; Koscher, B. A.; Eaton, S. W.; Yang, P.; Alivisatos, A. P. Highly Luminescent Colloidal Nanoplates of Perovskite Cesium Lead Halide and Their Oriented Assemblies. *J. Am. Chem. Soc.* **2015**, *137* (51), 16008–16011. https://doi.org/10.1021/jacs.5b11199.

(83) Shamsi, J.; Rastogi, P.; Caligiuri, V.; Abdelhady, A. L.; Spirito, D.; Manna, L.; Krahne, R. Bright-Emitting Perovskite Films by Large-Scale Synthesis and Photoinduced Solid-State Transformation of $CsPbBr_3$ Nanoplatelets. *ACS Nano* **2017**, *11* (10), 10206–10213. https://doi.org/10.1021/acsnano.7b04761.

(84) Grisorio, R.; Fanizza, E.; Allegretta, I.; Altamura, D.; Striccoli, M.; Terzano, R.; Giannini, C.; Vergaro, V.; Ciccarella, G.; Margiotta, N.; Suranna, G. P. Insights into the Role of the

Lead/Surfactant Ratio in the Formation and Passivation of Cesium Lead Bromide Perovskite Nanocrystals. *Nanoscale* **2020**, *12* (2), 623–637. https://doi.org/10.1039/C9NR08079A.

(85) Cho, J.; Jin, H.; Sellers, D. G.; Watson, D. F.; Son, D. H.; Banerjee, S. Influence of Ligand Shell Ordering on Dimensional Confinement of Cesium Lead Bromide ($CsPbBr_3$) Perovskite Nanoplatelets. *J. Mater. Chem. C* **2017**, *5* (34), 8810–8818. https://doi.org/10.1039/C7TC02194A.

(86) Shamsi, J.; Dang, Z.; Bianchini, P.; Canale, C.; Di Stasio, F.; Brescia, R.; Prato, M.; Manna, L. Colloidal Synthesis of Quantum Confined Single Crystal $CsPbBr_3$ Nanosheets with Lateral Size Control up to the Micrometer Range. *J. Am. Chem. Soc.* **2016**, *138* (23), 7240–7243. https://doi.org/10.1021/jacs.6b03166.

(87) Wang, Y.; Li, X.; Sreejith, S.; Cao, F.; Wang, Z.; Stuparu, M. C.; Zeng, H.; Sun, H. Photon Driven Transformation of Cesium Lead Halide Perovskites from Few-Monolayer Nanoplatelets to Bulk Phase. *Adv. Mater.* **2016**, *28* (48), 10637–10643. https://doi.org/10.1002/adma.201604110.

(88) Dang, Z.; Dhanabalan, B.; Castelli, A.; Dhall, R.; Bustillo, K. C.; Marchelli, D.; Spirito, D.; Petralanda, U.; Shamsi, J.; Manna, L.; Krahne, R.; Arciniegas, M. P. Temperature-Driven Transformation of $CsPbBr_3$ Nanoplatelets into Mosaic Nanotiles in Solution through Self-Assembly. *Nano Lett.* **2020**, *20* (3), 1808–1818. https://doi.org/10.1021/acs.nanolett.9b05036.

(89) Vonk, S. J. W.; Fridriksson, M. B.; Hinterding, S. O. M.; Mangnus, M. J. J.; van Swieten, T. P.; Grozema, F. C.; Rabouw, F. T.; van der Stam, W. Trapping and Detrapping in Colloidal Perovskite Nanoplatelets: Elucidation and Prevention of Nonradiative Processes through Chemical Treatment. *J. Phys. Chem. C* **2020**, *124* (14), 8047–8054. https://doi.org/10.1021/acs.jpcc.0c02287.

(90) Shamsi, J.; Kubicki, D.; Anaya, M.; Liu, Y.; Ji, K.; Frohna, K.; Grey, C. P.; Friend, R. H.; Stranks, S. D. Stable Hexylphosphonate-Capped Blue-Emitting Quantum-Confined $CsPbBr_3$ Nanoplatelets. *ACS Energy Lett.* **2020**, *5* (6), 1900–1907. https://doi.org/10.1021/acsenergylett.0c00935.

(91) Karmakar, A.; Dodd, M. S.; Zhang, X.; Oakley, M. S.; Klobukowski, M.; Michaelis, V. K. Mechanochemical Synthesis of 0D and 3D Cesium Lead Mixed Halide Perovskites. *Chem. Commun.* **2019**, *55* (35), 5079–5082. https://doi.org/10.1039/C8CC09622H.

(92) Piveteau, L.; Ong, T.-C.; Rossini, A. J.; Emsley, L.; Copéret, C.; Kovalenko, M. V. Structure of Colloidal Quantum Dots from Dynamic Nuclear Polarization Surface Enhanced NMR Spectroscopy. *J. Am. Chem. Soc.* **2015**, *137* (43), 13964–13971. https://doi.org/10.1021/jacs.5b09248.

Conspectus Graphic